Extreme Mechanics Letters 34 (2020) 100613

Contents lists available at ScienceDirect

Extreme Mechanics Letters

journal homepage: www.elsevier.com/locate/eml

Nanomechanical characterization of pressurized elastic fluid nanovesicles using indentation analysis

Xingyi Tang [a], Xinghua Shi [b], Yong Gan [c,d], Xin Yi [a,e,*]

[a] Department of Mechanics and Engineering Science, College of Engineering, Peking University, Beijing 100871, China
[b] CAS Key Laboratory for Nanosystem and Hierarchy Fabrication, CAS Center for Excellence in Nanoscience, National Center for Nanoscience and Technology, Chinese Academy of Sciences, Beijing 100190, China
[c] Shanghai Institute of Materia Medica, Chinese Academy of Sciences, Shanghai 201203, China
[d] University of Chinese Academy of Sciences, Beijing 100049, China
[e] Beijing Innovation Center for Engineering Science and Advanced Technology, Peking University, Beijing 100871, China

ARTICLE INFO

Article history:
Received 23 September 2019
Received in revised form 13 November 2019
Accepted 18 November 2019
Available online 21 November 2019

Keywords:
Indentation
Nanovesicles
Osmotic pressure
Young's modulus
Stiffness

ABSTRACT

Mechanical properties play fundamental roles in regulating the biological behaviors of nanovesicles in a wide range of implications including cell uptake, intercellular communication and developing nanocarriers for drug delivery. Here we theoretically probe the mechanical properties of nanovesicles using indentation analysis based on a minimal model fully accounting for both small and large indentation without introducing unphysical contact and geometrical conditions. Two types of vesicles are considered: one having a fixed area and the other undergoing areal stretch. The indentation response of pressurized elastic fluid vesicles depends on the membrane bending rigidity, osmotic pressure, adhesion energy and size of the indenter tip. Moreover, the osmotic pressure dominates the indentation response, effective stiffness and Young's modulus for strongly pressurized vesicles. An analytical and universal relation which offers a new and easy way to determine the osmotic pressure from the measured indentation force–depth curve is identified. Effects of the nanovesicle size on the effective stiffness at finite and zero osmotic pressures are analyzed and show significantly different trends. Further discussion is made on the differences between the indentation of fluid vesicles and solid thin shells.

1. Introduction

Nanovesicles with a hollow interior compartment surrounded by a fluidic lipid membrane can be treated as an elastic fluid thin shell structure, and could undergo large to extreme deformation in response to internal and external loading of small magnitude. With high adaptability in mechanical and physicochemical responses to external stimuli, nanovesicles (*e.g.* nanosized liposomes, extracellular vesicles, and endo/lysosomes) function not only in many cell activities including cell uptake, intercellular trafficking and communication [1–4], but also as prospective vehicles for the targeting in drug delivery and therapeutics [4–8]. For example, exosomes secreted from oral epithelial cells into saliva via exocytosis, have abundant tumor-antigen and function as biomarkers of the oral-cancer [5]. An exosomes-based delivery system is expected as a versatile strategy to treat inflammatory and neurodegenerative disorders such as a Parkinson's disease [8].

Mechanical properties so far have been recognized as important aspects in regulating the biological behaviors of nanoparticles in cell uptake, drug delivery and cytotoxicity. For examples, a complete cell membrane wrapping of a softer nanovesicle requires more adhesion energy than that of a stiffer vesicle [2,3]. Stiffness-dependent intracellular accumulation is observed for elastic nanoparticles [4,9,10]. Compared with solid capsules, nanovesicles of good flexibility exhibit good therapeutic efficacy [11]. Recently, it is found that exosomes derived from erythrocytes in hereditary spherocytosis have significantly different mechanical properties compared with these in the healthy situation [12]. This result suggests that mechanical properties of exosomes can be used as important parameters to characterize and diagnose diseases. Therefore, determination of the mechanical properties of nanovesicles becomes a key step in understanding the biological functions of nanovesicles and developing rational drug delivery strategies.

In comparison with approaches such as micropipette aspiration and thermal fluctuation which function well in optical observation at micro- and larger scales and less suitable for

* Corresponding author at: Department of Mechanics and Engineering Science, College of Engineering, Peking University, Beijing 100871, China.
E-mail address: xyi@pku.edu.cn (X. Yi).

https://doi.org/10.1016/j.eml.2019.100613
2352-4316/

nanovesicles, nanoindentation measurement has been demonstrated to be a valuable approach to capture the apparent mechanical properties of vesicles at nanoscale [13–16]. However, the reported experimental data exhibit large scatter. One of the possible reasons is that post-processing of these nanoindentation analyses is based on the classical contact mechanics modeling such as the Hertz contact theory [17], which shall be more suitable for solid materials rather than elastic fluid structures such as lipid vesicles. Moreover, a rational modeling of the nanovesicle indentation is complicated by a precise characterization of the configuration of the largely deformed vesicle and the vesicle–indenter and vesicle–substrate contact conditions, and so far a robust modeling without unphysical assumptions on the configuration and contact conditions of the deformed nanovesicle is lacked.

In this study, we theoretically analyze the mechanical behaviors of pressurized elastic fluid nanovesicles upon indentation by a rigid parabolic indenter. Characterizing the vesicle deformation through a combination of the angle-arclength parametrization and numerical optimization approach, a minimal model is developed fully taking into account both small and large indentation with explicit consideration of the vesicle–indenter contact and vesicle–substrate contact. We systematically analyze how the indentation force–depth curves are affected by the membrane bending rigidity, osmotic pressure, adhesion energy and indenter size. The effective stiffness and Young's modulus of the vesicle are determined. A linear relation correlating the slope of the force–depth curve to the osmotic pressure at sufficiently large depth is identified. Shedding light on the mechanical behaviors of nanovesicles upon compressive external stimuli, our results may have important implications in nanovesicle-based drug delivery.

2. Modeling and method

We consider the indentation of a spherical lipid nanovesicle with an osmotic pressure Δp adhering on a rigid flat substrate. The axisymmetric deformation of the vesicle is assumed as illustrated in Fig. 1. The system is divided into three regions: the indenter tip-vesicle contact region, the outer free vesicle region, the vesicle–substrate contact region. Hereinafter, quantities pertaining to these three regions in sequence are identified by subscripts 1, 2 and 3, respectively.

In this work, we focus on two different types of vesicles of zero spontaneous curvature. The vesicle of the first type is assumed to have a fixed total surface area $A(=4\pi R^2)$ and its bending deformation obeys the Canham–Helfrich model [18]. Therefore, the total system energy at the indentation depth Δh is described by the Helfrich functional as [19–21]

$$E_{\text{tot}} = 2\kappa \int M_1^2 \mathrm{d}A_1 + 2\kappa \int M_2^2 \mathrm{d}A_2 - \Delta p(V - V_0) - \gamma A_3,$$

where κ is the membrane bending rigidity, M_i and $\mathrm{d}A_i$ $(i = 1, 2)$ are the mean curvature and surface element of the vesicle in regions 1 and 2, respectively; $V_0(=4\pi R^3/3)$ and V are the original and deformed volumes of the vesicle under the pressure difference Δp between the interior and exterior of the vesicles; $\gamma(>0)$ is the adhesion energy and A_3 the surface area of the vesicle-substrate contact region. The total surface area is fixed as $\sum_{i=1}^{3} A_i = A$. The adhesive interaction between the indenter tip and vesicle is assumed to be negligible. Here we focus on the case of fixed pressure difference, which is valid for vesicles of high water permeability or indentation of a long time scale. For vesicles of low water permeability or in the case of a fast indentation with a compression process less than few seconds, the vesicle volume is more appropriately to be approximated as constant since the water permeation across the membrane is much slower compared with the compression process [22].

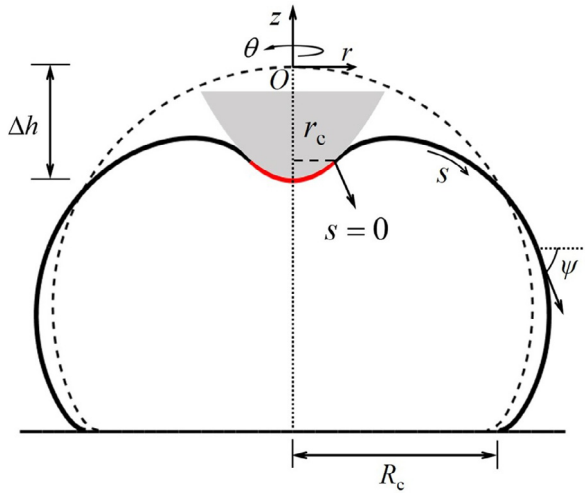

Fig. 1. Indentation of a pressurized nanovesicle by a parabolic indenter tip (gray region) in a cylindrical coordinate (r, θ, z) with the region of contact between the vesicle and indenter tip depicted by a red curve. In the outer free vesicle region, the arclength s is defined along the vesicle meridian originating from the edge of contact $(r = r_c)$ between the indenter tip and vesicle to the vesicle-substrate contact edge $(r = R_c, \psi = -\pi)$. In our notation, the tangent angle ψ is negative as it is measured clockwise from the positive r-axis and ψ is required to be equal to $-\pi$ at the bottom contact edge to enforce the angle continuity. The dashed line depicts the configuration of the vesicle in the absence of indentation. The indentation depth $\Delta h(>0)$ denotes the distance between the tip apex and north pole of the vesicle before indentation.

In comparison with the first vesicle type considered above, the vesicle of the second type is subject to area stretch. In the case of uniform areal stretch $(A - A_0)/A$ with $A_0(=4\pi R^2)$ and A as the areas of the original and deformed vesicle, the total free energy of this system is

$$E_{\text{tot}} = 2\kappa \int M_1^2 \mathrm{d}A_1 + 2\kappa \int M_2^2 \mathrm{d}A_2 + \frac{K_A}{2}\frac{(A - A_0)^2}{A_0} - \Delta p(V - V_0) - \gamma A_3,$$

where K_A is the area compression modulus and has characteristic values in the range 0.08 N/m–0.2 N/m [23].

Assuming the axisymmetric indenter of a parabolic shape with a radius of curvature R_t at the apex, the parabolic region of the indenter is described by

$$h_c = \frac{r_c^2}{2R_t},$$

where r_c and h_c are the contact radius and depth, respectively. The tangent angle ψ_c at the tip-vesicle contact edge is determined by $\tan\psi_c = r_c/R_t$. The characteristic tip radius R_t is in the range of 5 nm to 40 nm.

From simple geometrical arguments, we can obtain the volume of the indenter tip in contact with the vesicle as

$$V_1 = \frac{\pi r_c^2 h_c}{2} = \frac{\pi r_c^4}{4R_t},$$

the corresponding contact surface area as

$$A_1 = \frac{\pi r_c}{6h_c^2}[(r_c^2 + 4h_c^2)^{3/2} - r_c^3] = \frac{2\pi R_t^2}{3}\left[\left(1 + \frac{r_c^2}{R_t^2}\right)^{3/2} - 1\right],$$

and the bending energy of the vesicle membrane in region 1 as

$$E_1 = 2\kappa \int M_1^2 \mathrm{d}A_1 = \frac{\pi\kappa}{3}\left[4 + \frac{3r_c^4/R_t^4 - 4}{(1 + r_c^2/R_t^2)^{3/2}}\right]$$

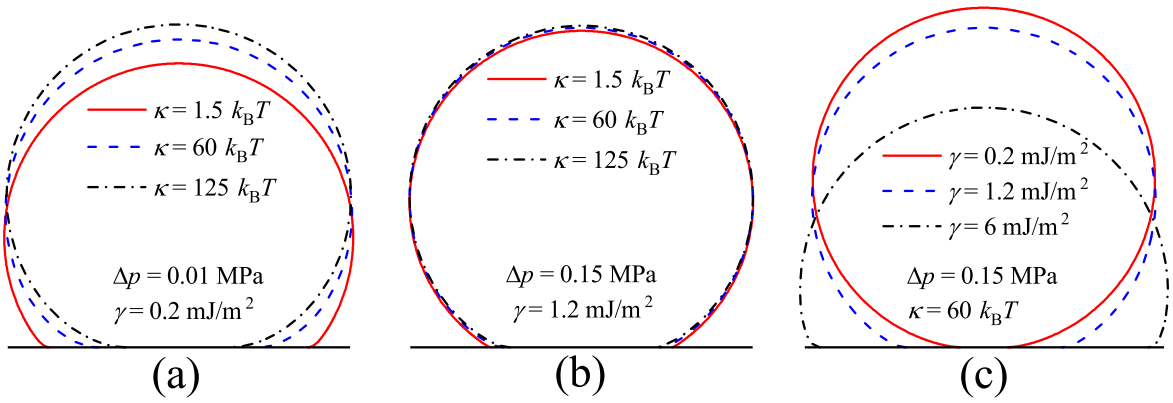

Fig. 2. Initial equilibrium configurations of vesicles with $R = 100$ nm at different values of the membrane bending rigidity κ with small and large osmotic pressure Δp (a,b), and adhesion energy γ (c).

with the local mean curvature $M_1 = (r^2 + 2R_t^2)/[2(r^2 + R_t^2)^{3/2}]$.

The configuration of the free vesicle region is characterized by the tangent angle ψ and arclength s with geometric relations $\mathrm{d}r/\mathrm{d}s = \cos\psi$ and $\mathrm{d}z/\mathrm{d}s = \sin\psi$, and the mean curvature is $M_2 = (\mathrm{d}\psi/\mathrm{d}s + \sin\psi/r)/2$. Therefore, the membrane bending energy in region 2 is

$$E_2 = 2\kappa \int M_2^2 \mathrm{d}A_2 = \pi\kappa \int_0^{l_2} r\left(\frac{\mathrm{d}\psi}{\mathrm{d}s} + \frac{\sin\psi}{r}\right)^2 \mathrm{d}s,$$

where s, r and l_2 are the arclength, radial coordinate and undetermined total arclength of the free vesicle region, respectively. The volume V of the deformed vesicle is

$$V = -V_1 - \pi \int_0^{l_2} r^2 \sin\psi \mathrm{d}s,$$

and the area of the free vesicle is $A_2 = 2\pi \int_0^{l_2} r\mathrm{d}s$.

In the vesicle-substrate contact region, the membrane bending energy is zero as the membrane is flat, and the contact area is $A_3 = \pi R_c^2$ with $R_c = r_c + \int_0^{l_2} \cos\psi \mathrm{d}s$ as the radius of the vesicle-substrate contact region.

Once the vesicle configuration is determined, the system energy E_{tot} can be obtained. In the free vesicle region, E_{tot} is represented as a function of ψ approximated by a cubic B-spline curve as $\psi(t) = \sum_{i=0}^{n} a_i N_i(t)$. Here the variable t is defined as $t = s/l_2$ such that $t = 0$ at the tip-vesicle contact edge and $t = 1$ at the vesicle-substrate contact edge as the total arclength l_2 of the free vesicle region is unknown. In the above representation of $\psi(t)$ by a B-spline curve, a_i denotes control points and $N_i(t)$ is the basic function defined recursively following the de Boor algorithm [24] on a location vector $T = \{t_0, \ldots, t_j, \ldots, t_{n+4}\}$ containing $n+5$ elements in a non-descending order $t_j \le t \le t_{j+1}$. The locations t_j are called knots with $j(= 0, 1, \ldots, n+4)$ as the knot index, and the location vector T as a set of coordinates in the parametric space is called knot vector. As the vesicle deformation might be relatively large in the vicinities of the indenter tip and the vesicle–substrate contact edge, a non-uniform knot vector is introduced with smaller knot distances $t_{j+1} - t_j$ at small and large j. Moreover, $t_j = 0$ $(j = 0, \ldots, 3)$ and $t_j = 1$ $(j = n+1, \ldots, n+4)$ are specified for the non-periodic B-spline curve here.

At a given indentation depth Δh, the minimum energy state of the vesicle is numerically determined employing the interior point optimization technique, in which the first and second derivatives of E_{tot} as well as the necessary inequality or equality constraints with respect to parameters a_i, r_c and l_2 are required. In our case, inequality constraints that the indenter tip surface has a larger z-coordinate than that of the vesicle are introduced to prevent penetration between the vesicle and indenter tip. Other boundary conditions include the continuities of the angle ψ and the r- and z-coordinates at the top and bottom contact edges ($t = 0$ and 1). For example, $\psi(t = 0) = \arctan(r_c/R_t)$ and $\psi(t = 1) = -\pi$, requiring $a_0 = \arctan(r_c/R_t)$ and $a_n = -\pi$. For the first type vesicle, the fixed vesicle area $A = A_1 + A_2 + A_3$ behaves as an additional equality constraint. Once all required first and second derivatives are obtained, the minimized energy E_{tot} can be determined using the interior point method. With the knowledge of $E_{tot}(\Delta h)$, the effective axial indentation force F can be given from $F(\Delta h) = \mathrm{d}E_{tot}/\mathrm{d}(\Delta h)$, and then the effective (or apparent) stiffness and Young's modulus can be determined.

3. Results

We first probe the equilibrium configurations of pressurized nanovesicles before indentation (Fig. 2). The nanovesicle is of radius $R = 100$ nm at different values of bending rigidity κ, osmotic pressure Δp, and adhesion energy γ. As κ or Δp decreases and γ increases, the vesicle undergoes deformation of an increasing extent as expected.

The equilibrium configurations of pressurized nanovesicles with $R = 100$ nm and $\kappa = 240$ pN· nm at different indentation depths $\Delta h/R$ are shown in Fig. 3. As Δh increases, the region of contact between the substrate and vesicle increases, and the vesicle undergoes shape transformation from an approximately spherical cap to a concave shape. Decreasing Δp leads to a more flattened vesicle configuration as the vesicle becomes more flexible at a lower Δp. Increasing γ also leads to a more flattened vesicle with a larger area of contact between the vesicle and substrate. At relatively large Δp, the vesicle configuration is insensitive to κ but more sensitive to Δp and γ (Figs. 2 and 3). This feature is also reflected in the indentation force–depth curves (Fig. 4).

To investigate the mechanical behaviors of the pressurized nanovesicle upon indentation, we investigate the relation between the axial indentation force F and the indentation depth Δh (Fig. 4). It is shown that the slope of the force curve $\mathrm{d}F/\mathrm{d}(\Delta h)$ increases as Δh increases, which is due to the more significant vesicle deformation at a larger Δh. For a vesicle of a given size, its deformation upon indentation depends together on κ, Δp, γ and R_t. Therefore, we propose to identify and analyze their individual effects on the F–Δh relation. Fig. 4a shows that the membrane bending rigidity κ has a minor effect on the F–Δh curve at relatively large Δp. Moreover, the adhesion energy plays an important role and the osmotic pressure Δp plays a more significant role in regulating the indentation force profile while noting that larger Δp and γ correspond to larger indentation force (Fig. 4b and c). The osmotic effect on the F–Δh curves in Fig. 4b is consistent with experimental studies on the indentation of MDCK-II

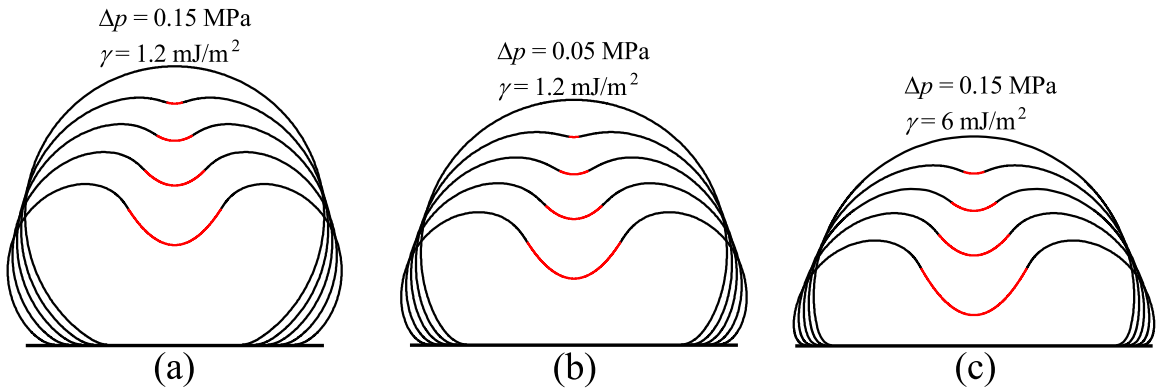

Fig. 3. Equilibrium configurations of pressurized nanovesicles with radius $R = 100$ nm and bending rigidity $\kappa = 240$ pN· nm at different normalized indentation depths $\Delta h/R = 0, 0.25, 0.5, 0.8$ and 1.2. Three parameter sets of $(\Delta p, \gamma)$ are considered: (a) $\Delta p = 0.15$ MPa, $\gamma = 1.2$ mJ/m^2, (b) $\Delta p = 0.05$ MPa, $\gamma = 1.2$ mJ/m^2, (c) $\Delta p = 0.15$ MPa, $\gamma = 6$ mJ/m^2. The indenter tip of $R_t = 20$ nm is not shown for clarity. Red curves represent the indenter tip-vesicle contact regions.

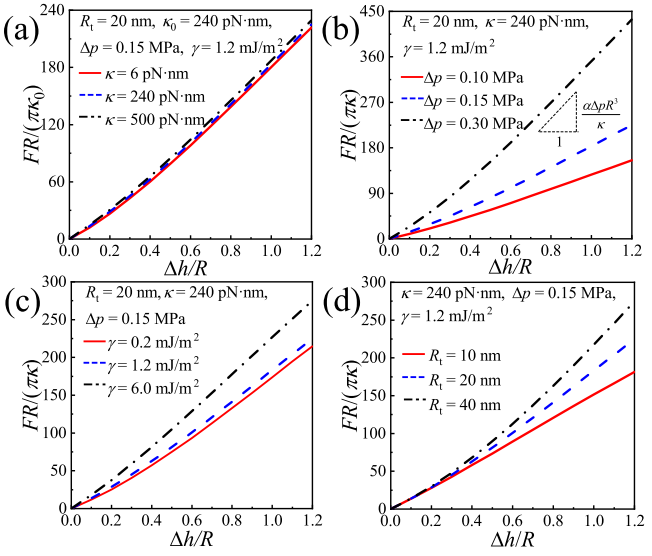

Fig. 4. Effects of the membrane bending rigidity κ (a), osmotic pressure Δp (b), adhesion energy γ (c) and tip radius R_t (d) on the indentation force–depth curves.

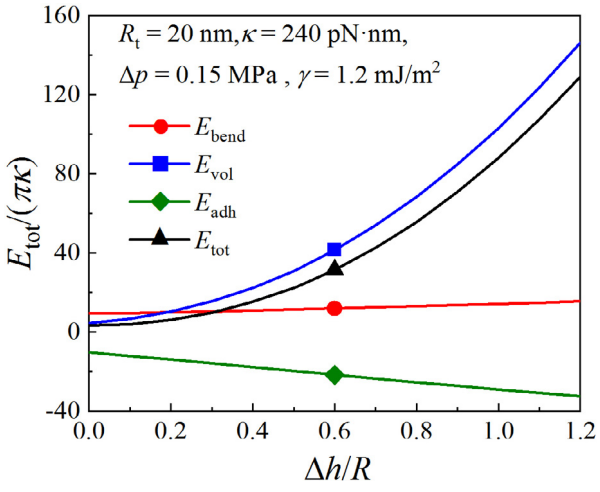

Fig. 5. Variations of E_{tot} of the first type vesicle with $R = 100$ nm and its three components as a function of the indentation depth Δh at $R_t = 20$ nm, $\kappa = 240$ pN· nm, $\Delta p = 0.15$ MPa and $\gamma = 1.2$ mJ/m^2 ($\bar{p} \equiv \Delta p R^3/\kappa = 625, \bar{\gamma} \equiv \gamma R^2/\kappa = 50$). Here $E_{tot} = E_{bend} + E_{vol} + E_{adh}$ with the bending energy as $E_{bend} = 2\kappa \int M_1^2 dA_1 + 2\kappa \int M_2^2 dA_2$, the vesicle volume associated term $E_{vol} = -\Delta p(V - V_0)$ and the adhesion energy $E_{adh} = -\gamma A_3$.

kidney cells under the different osmotic conditions [25]. We also investigate the dependence of the indentation force F on the tip radius R_t. It is shown that F is directly proportional to R_t (Fig. 4d), consistent with experimental measurement [16,26].

A careful observation of Fig. 4b suggests that the F–Δh curves demonstrate a linear relationship at large Δh as

$$\mathrm{d}F \times \frac{R}{\pi\kappa} \sim \mathrm{d}(\Delta h) \times \frac{\alpha}{R}\frac{\Delta p R^3}{\kappa} \qquad \text{or} \qquad \frac{\mathrm{d}F}{\mathrm{d}(\Delta h)} \sim \alpha\pi\Delta p R,$$

where the parameter is $\alpha = 1/3$ insensitive to the adhesion energy γ, confirmed by further calculations. Taking advantage of this simple relation, for a strongly pressurized vesicle we can determine the osmotic pressure Δp from the measured F–Δh curve. Interestingly, a similar relation $\mathrm{d}F/\mathrm{d}(\Delta h) \sim \pi\Delta p R$ or $F \sim \pi\Delta p R \Delta h$ (with $\alpha = 1$) has been found in the case of indenting a pressurized linear elastic solid thin shell in the absence of adhesion energy [27].

The total system energy E_{tot} for the first type vesicle consists of three components: the bending energy $E_{bend} = 2\kappa \int M_1^2 dA_1 + 2\kappa \int M_2^2 dA_2$, the work done by the osmotic pressure $E_{vol} = -\Delta p(V - V_0)$, and the adhesion energy $E_{adh} = -\gamma A_3$. To illustrate the contribution of each energy component to E_{tot}, we plot the total energy E_{tot} and its three components as functions of the indentation depth Δh (Fig. 5). Our case study at $\Delta p = 0.15$ MPa and $\gamma = 1.2$ mJ/m^2 indicates that E_{vol} plays the most important role among these three components and E_{bend} plays a minor role in regulating the vesicle indentation from an energetic point of view. These features are consistent with the F–Δh curves in Fig. 4 showing that F is insensitive to κ but strongly depends on Δp.

The conclusion that the variation of the total energy E_{tot} during the vesicle indentation is primarily owing to E_{vol} rather than E_{bend} can also be drawn based on a simple analysis as follows [28]. Imagine that the top portion of a height h of the spherical vesicle is flattened and assume that the rest part of the vesicle remains as a spherical cap. The surface area and the volume of the flattened spherical top portion is $2\pi Rh$ and $\pi h^2(3R - h)/3$, respectively. As the membrane bending energy change per unit area is $2\kappa/R^2$, the variation of E_{bend} has a magnitude of $4\pi\kappa h/R$ and the work of Δp is the pressure times the volume change as $\Delta p\pi h^2(3R - h)/3$. Therefore, the ratio of the work done against the membrane bending to that against the pressure is $12\kappa/[\Delta p R h(3R - h)]$, which is about 0.0154 for $\kappa = 240$ pN· nm, $\Delta p = 0.15$ MPa, $R = 100$ nm and $h = 50$ nm.

With knowledge of the F–Δh curves in Fig. 4, the slope $K \equiv \mathrm{d}F/\mathrm{d}(\Delta h)$ is adopted to characterize the effective vesicle stiffness.

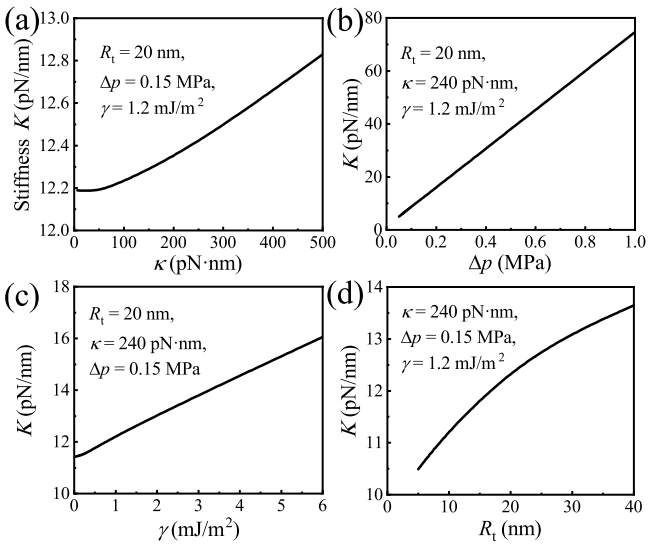

Fig. 6. Effective stiffness K the nanovesicle as functions of the membrane bending rigidity κ (a), osmotic pressure Δp (b), adhesion energy γ (c) and indenter tip radius R_t (d).

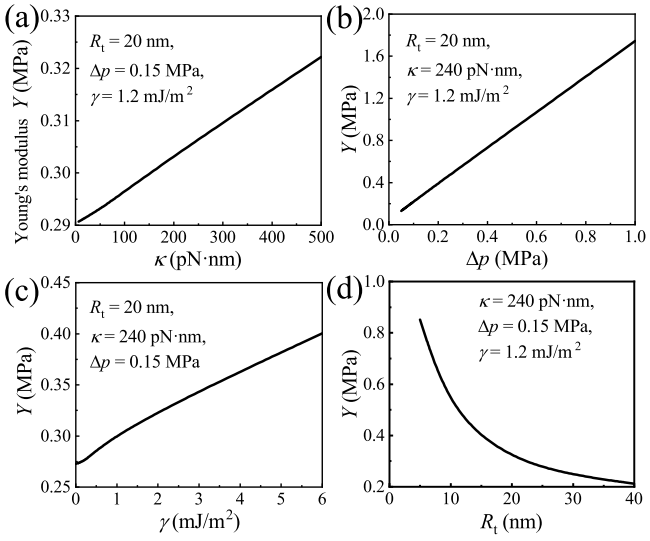

Fig. 7. Effective Young's modulus Y of the nanovesicle as functions of κ (a), Δp (b), γ (c) and R_t (d).

In the present study, we fit the F–Δh curves in the range of $\Delta h/R$ from 0.2 to 0.3 by a linear function and define its slope as the effective vesicle stiffness K. Fig. 6a shows that the vesicle stiffness K is nearly a constant at small κ, while K is almost linearly proportional to κ of a relatively large value (*e.g.* κ >100 pN· nm here). Similar linear proportionality could also be found in the K–Δp and K–γ relations (Fig. 6b and c). Comparing the magnitudes of the curve slopes in Fig. 6a–c, one can draw a conclusion that the osmotic pressure Δp is a dominant variable on the vesicle stiffness, consistent with our analysis on Figs. 4 and 5. The simulated vesicle stiffness K also exhibits size-dependence on the tip radius R_t. A larger R_t corresponds to a larger K (Fig. 6d).

Another featured parameter for the vesicle rigidity is the effective Young's modulus Y which is usually estimated based on the continuum contact mechanics modeling [17]. The classical Hertz contact theory is developed for indentation much smaller than the indenter tip radius, and cannot be directly employed for soft materials including vesicles undergoing large deformation upon indentation. To achieve a more sound estimation on the effective Young's modulus of vesicles undergoing finite deformation, here we adopt the Sneddon theory which does not require the condition of indentation much smaller than the tip radius [29–31].

Assuming the Poisson ratio ν = 0.5, we can calculate the Young's modulus Y at a given Δh according to the Sneddon theory [29,30] as

$$F = \frac{Y}{1-\nu^2}\left[(R_t^2 + a^2)\frac{\Delta h}{a} - aR_t\right],$$

where a is the apparent contact radius determined by the indentation depth Δh and the tip radius R_t via the relation $\Delta h = (a/2)\ln[(R_t + a)/(R_t - a)]$. In the following analysis, the effective Young's modulus Y of the vesicle is taken at $\Delta h = 0.3R$.

The dependence of the effective Young's modulus Y and the stiffness K on κ, Δp and γ is quite similar (comparing Fig. 6a–c with Fig. 7a–c). As shown in Fig. 6d, the estimated vesicle stiffness K is significantly affected by tip size. It is more intriguing that the estimated stiffness K increases as the tip size R_t increases, while the effective Young's modulus Y decreases as R_t increases (Figs. 6d and 7d). The trend of Y–R_t curve is also obtained using the Hertz theory while we keep in mind that the Hertz theory is not applicable in the current case of soft vesicles. The significant contrast between the K–R_t and Y–R_t profiles in our theoretical analysis is consistent with experimental studies on the indentation of tomato mesocarp cells which show that the measured Young's modulus of the cell increases but the stiffness decreases as the indenter tip size becomes smaller [26].

An explanation for this slightly counterintuitive phenomenon is offered as follows. As the tip radius R_t increases, the indenter tip becomes more flattened and the indenter force F at the same indentation depth increases, which leads to a larger vesicle stiffness K of $K \sim F \sim R_t^{\beta}$ with β as a positive geometry parameter. Based on the contact mechanics theory, Y is proportional to F but inversely proportional to the tip size or radius R_t. A competition between the force F and the geometry factor R_t leads to a decreasing Young's modulus Y of the vesicle as R_t increases, that is, $Y \sim R_t^{-\beta}$. The above discussion can be readily illustrated using the analytical solution on the non-adhesive contact between a rigid spherical indenter and an elastic half-space [17,32]. For a rigid spherical tip of radius R_t indenting an elastic isotropic half-space of a Young's modulus Y and Poisson ratio ν, the indentation force F at the depth Δh is given as $F = 4Y'R_t^{1/2}(\Delta h)^{3/2}/3$ with $Y' = Y/(1-\nu^2)$, which leads to $K = \mathrm{d}F/\mathrm{d}(\Delta h) = 3F/(2\Delta h)$ and $Y' = 3FR_t^{-1/2}(\Delta h)^{-3/2}/4$, or in a scaling form as $K \sim R_t^{1/2}$ and $Y \sim R_t^{-1/2}$.

For a strongly pressurized vesicle, the effective stiffness K decrease with increasing vesicle radius R; while for a nonpressurized vesicle, K increases as R increases (Fig. 8), which is consistent with reported experimental results on the indentation of nanosized dimyristoyl-phosphatidylcholine (DMPC) liposomes at a small osmotic pressure estimated around tens of kPa [14].

For the second type of vesicle taking into account the membrane area stretch, we perform case studies on the effect of the area compressibility modulus K_A on the indentation force–depth curve. Characteristic values of K_A fall in the range of 0.08 N/m to 0.2 N/m [23]. Though the total free energy E_{tot} strongly depends on K_A (Fig. 9a), K_A in a biological range has infinitesimal effects on the indentation force–depth curves (Fig. 9b). In addition to the bending energy E_{bend}, the vesicle volume associated term E_{vol} and the adhesion energy E_{adh} as related with the free energy of the first type vesicle, the stretching energy E_{str} contributes to the total energy E_{tot} of the second type vesicle. Further calculations indicate that the variation of E_{vol} as a function of Δh has significant influence, the variations of E_{str} and E_{adh} have minor effects, and the variation of E_{bend} has the least effect on the evolution of $E_{tot}(\Delta h)$ (see Fig. 10).

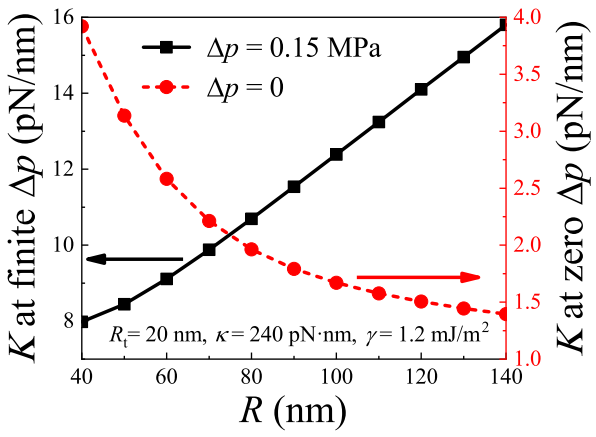

Fig. 8. Effects of the nanovesicle size on the effective stiffness K at finite and zero Δp.

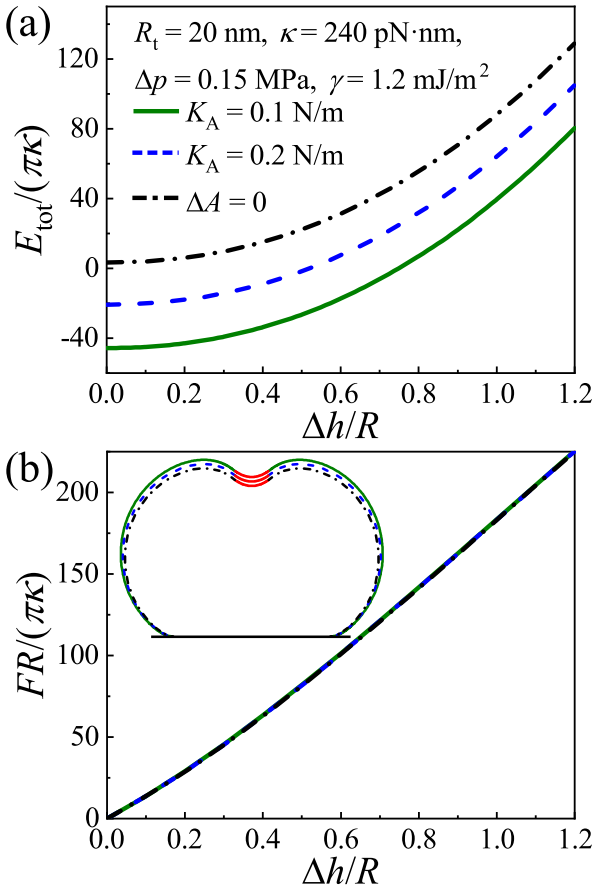

Fig. 9. Effects of the area compression modulus K_A on the total free energy (a) and the indentation force–depth curves (b). Two different values of K_A (0.1 N/m and 0.2 N/m) are considered in comparison with the case of the first type vesicle of a fixed area ($\Delta A = A - A_0 = 0$) or equivalently an infinitely large K_A.

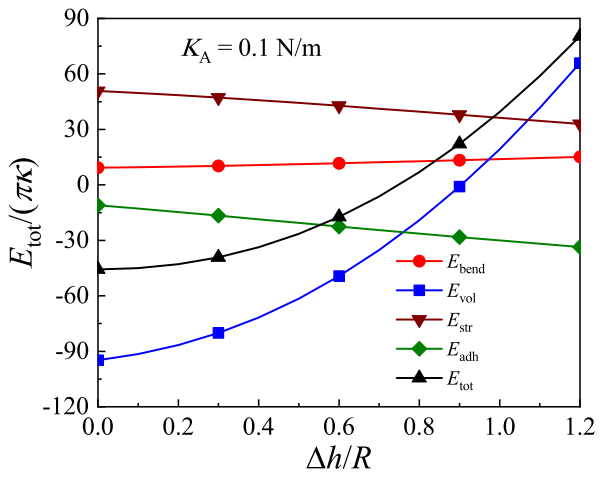

Fig. 10. Variations of the total free energy E_{tot} of the second type vesicle ($R = 100$ nm, $K_A = 0.1$ N/m) and its four components as a function of the indentation depth Δh at $R_t = 20$ nm, $\kappa = 240$ pN· nm, $\Delta p = 0.15$ MPa, and $\gamma = 1.2$ mJ/m^2 ($\bar{p} \equiv \Delta p R^3/\kappa = 625$, $\bar{\gamma} \equiv \gamma R^2/\kappa = 50$). Here $E_{tot} = E_{bend} + E_{str} + E_{vol} + E_{adh}$ with the bending energy as $E_{bend} = 2\kappa \int M_1^2 dA_1 + 2\kappa \int M_2^2 dA_2$, the stretching energy $E_{str} = K_A(A - A_0)^2/(2A_0)$, the work done by the osmotic pressure $E_{vol} = -\Delta p(V - V_0)$, and the adhesion energy $E_{adh} = -\gamma A_3$.

4. Discussion

Upon indentation and adhesive interaction with the substrate, the vesicle evolves from an initial spherical shape to a strongly curved configuration with overhang profile segments which cannot be fully described as a whole by a Monge parametrization. To characterize the deformed vesicle, theoretical models in previous literature approximate the free part of the vesicle as a spherical cap in the case of strong vesicle-substrate adhesion or through a combination of several spherical caps [33]. To simplify the contact conditions, a local point force has been used in existing literature to model the contact between the indenter tip and vesicle and the vesicle-substrate contact is ignored [16]. In our current study, the vesicle configurations at both small and large indentation depths are fully described using the angle-arclength parametrization, which enables us to characterize the overhang profile segments and integrate the precise boundary conditions of the contact between the indenter tip and vesicle and that between the vesicle and substrate.

In the current study, we model the vesicle with a lipid membrane in a fluidic state with the classical Canham–Helfrich membrane theory [18], which is based on the facts that the lipid molecules undergo free lateral movement and the membrane is of high resistance to lateral stretching. Therefore, the membrane stretching if incorporated is uniform and independent of the local position in the lipid membrane at equilibrium as we adopted. In addition to vesicles, capsules such as polymeric capsules, polymeric micelles and viral capsids are elastic solid thin shells from a mechanical point of view and they serve as another important type of soft particles with broad biomedical applications, especially in the fields of drug delivery and diagnostics. For a solid thin shell subject to vertical indentation, the strain field is not uniform and the stretch along the longitudinal and circumferential directions are different. The high energetic cost of circumferential stretch associated with the flattening of the curved shell leads to a significantly larger indentation stiffness than that of the vesicle with a comparable bending rigidity. Moreover, the solid thin shell could exhibit different types of mechanical instabilities such as buckling and wrinkling as a manner of releasing strain energy by relieving the circumferential compression through bending [27,34–36], which cannot be observed in the indentation of a vesicle due to the fluidic feature of the lipid membrane. For example, gel phase vesicles, rather than the fluid phase vesicles, subject to osmotic shock could develop complex morphological changes including bowl-like conformations along with buckling instability owing to the solid elastic nature of the gel phase membranes [34]. Long-range strong adhesion between a spherical thin elastic shell and a flat rigid substrate can induce possible wrinkling in the shell near the contact edge and the inversion buckling of the central

adhesion region of the shell away from the substrate [35]. The indentation of a pressurized linear elastic shell could induce a wrinkling instability as the indentation depth increases [36] and the relationship between the indentation force and depth demonstrates two linear regimes [27]. The solid nature of the capsule shell and the consequent anisotropic and non-uniform stretch lead to much higher energy cost of the capsule deformation in comparison to the fluid lipid vesicles [37]. Therefore, modeling fluid phase vesicles using the elastic thin shell theory would significantly overestimate the stiffness and Young's modulus of the vesicle. For the vesicles with an interior actin cortex lying immediately beneath the membrane, a two-layer model considering the fluid lipid membrane and solid cortex shell shall be more appropriate.

Besides the axisymmetric parabolic indenter we consider here, another kind of axisymmetric indenters widely used has a cylindrical tip. At intermediate and deep indentation depths Δh, the radius of the circular edge of contact between the tip and vesicle would main the same value as that of the cylindrical tip. This geometric feature of contact is strikingly different from the case of the indentation by a parabolic indenter in which the size of contact edge continuously increases as Δh increases. Our recent theoretical study on the vesicle indentation by a rigid cylindrical indenter indicates that as Δh increases the indentation force F increases to a peak value, then drops steeply and almost saturates at a certain value upon the formation of an inward tubular membrane protrusion [21]. A relevant experimental work exhibiting an inward tubulation is pulling a vesicle toward its interior by pressing a trapped bead [38]. It is shown that the indented vesicle maintains its configuration as a spherical cap along the formation of an inward membrane nanotube [38]. The formation of long cylindrical tubular structures is commonly observed for fluidic lipid membranes subject to a localized force or displacement [38–40] but is suppressed for solid elastic thin shells due to the high energetic cost of in-plane stretching. As a result, only a relatively short tubular structure could be possibly observed for the soft solid shell at a large indentation depth and moreover there always exists in the shell a highly deformed outer free region with a size significantly larger than the indenter radius at the base of the cylindrical indenter [27,41,42].

For a strongly pressurized elastic fluid lipid vesicle of radius R, our results indicate that the slope of the F–Δh curve at sufficiently large Δh exhibits a linear relationship with the osmotic pressure Δp as $\mathrm{d}F/\mathrm{d}(\Delta h) \sim \alpha\pi\Delta pR$ with $\alpha = 1/3$. A similar relation with $\mathrm{d}F/\mathrm{d}(\Delta h) \sim \pi\Delta pR$ with $\alpha = 1$ has been found for a pressurized linear elastic solid thin shell [27]. It seems that α depends on and might be assigned as a featured parameter to characterize the physical nature of the shell structures in the indentation analysis. Related veiled questions include the determination of α for vesicles in gel phase and solid capsules of other types of constitutive relations even with consideration of the effects of the membrane/shell thickness and viscosity. It will be interesting and might be challenging to conduct a thorough theoretical analysis on these aspects in the future.

Though lipid vesicles have been widely used as a minimal biomimetic model of cells to probe the mechanical and biophysical features of certain cellular activities such as membrane tubulation and endocytosis, several key differences between lipid vesicles and animal cells limit the applicability of the current theoretical results to measuring mechanical properties of living cells from mechanical and biophysical viewpoints. One significant difference is that lipid vesicles have no cellular organelles such as nucleus and mitochondria, which could give rise to much larger stiffness for cells upon a deep indentation. Moreover, cells undergo shape and volume change regulated by the dynamic cytoskeletal network [43] and passive or active ion channels [44], which could lead to rheological behaviors and rate-dependent responses of cells under distinct loading conditions. There are also some special cases that the current model about nanovesicle indentation can be generalized and become applicable in measurement of cellular mechanical properties. For example, mature red blood cells, with spectrin network attached to the membrane but lacking cell nucleus and most organelles, can be modeled by a lipid vesicle of a given reduced volume with actin-based cortex (regarded as a elastic solid layer with pre-stress) assembled at the inner leaflet of the vesicle. In short words, stiffness or Young's modulus alone is not adequate to capture the mechanical properties of living cells. Depending on cell types more sophisticated models taking into account cytoskeleton mechanics, rate-dependent behaviors and active cellular forces are required in the determination of cell properties.

5. Conclusions

We theoretically investigate the mechanical properties of pressurized nanovesicles using indentation analysis. In this study, two types of vesicles are considered, one with a prescribed area constraint and the other subject to uniform area stretch. Using the angle-arclength parametrization, the vesicle configurations at small and large indentation depths and the boundary conditions of the contact between the indenter tip and vesicle and that between the vesicle and substrate are appropriately integrated. The indentation force–depth curves as well as the effective stiffness and Young's modulus of the nanovesicles at different osmotic pressures Δp, membrane bending rigidities κ, adhesion energy γ of the substrate-vesicle interface and indenter tip sizes are determined. A larger vesicle stiffness is expected at larger Δp, κ and γ. It is found that the osmotic pressure dominates the effective stiffness or Young's modulus of a pressurized nanovesicle over the membrane bending rigidity, consistent with the energetic analysis. A linear relation correlating the slope of the indentation force–depth curve to the osmotic pressure Δp of the vesicle at sufficiently large depth is identified, which offers a new way to determine Δp from the measured force–depth data. At finite and zero osmotic pressures, the vesicle stiffness increases and decreases, respectively, as the vesicle size increases. Our results show that tuning the osmotic pressure of vesicles is an effective way to regulate the mechanical behaviors of the inter- and intracellular nanovesicles which are widely used or encountered in cell uptake, medical diagnostics, intercellular communication and drug delivery.

Our theoretical approach is readily extended to axisymmetric deformation of lipid membrane patches, gel phase vesicles, and solid thin shell structures [15,27,34,41,42]. The present analysis can serve as a foundation for future work on the cell membrane penetration by nanoprobes and nanoparticles with consideration of the microstructure of the deformed membrane [45–47] and on the indentation and extraction of vesicles and cells taking into account the viscosity associated with the membrane or the fluidic environment [48–50], water permeation [44], and the mechanical coupling between the cytoskeleton and membrane [33,43,51].

Declaration of competing interest

The authors declare that they have no known competing financial interests or personal relationships that could have appeared to influence the work reported in this paper.

Acknowledgments

This work was supported by the National Natural Science Foundation of China (Grant No. 11872005). Computation resources supported by the High-performance Computing Platform of Peking University are acknowledged.

References

[1] M. Colombo, G. Raposo, C. Théry, Biogenesis, secretion, and intercellular interactions of exosomes and other extracellular vesicles, Annu. Rev. Cell Dev. Biol. 30 (2014) 255–289, http://dx.doi.org/10.1146/annurev-cellbio-101512-122326.

[2] X. Yi, X. Shi, H. Gao, Cellular uptake of elastic nanoparticles, Phys. Rev. Lett. 107 (2011) 098101, http://dx.doi.org/10.1103/PhysRevLett.107.098101.

[3] J. Sun, L. Zhang, J. Wang, Q. Feng, D. Liu, Q. Yin, D. Xu, Y. Wei, B. Ding, X. Shi, X. Jiang, Tunable rigidity of (polymeric core)–(lipid shell) nanoparticles for regulated cellular uptake, Adv. Mater. 27 (2015) 1402–1407, http://dx.doi.org/10.1002/adma.201404788.

[4] A.C. Anselmo, S. Mitragotri, Impact of particle elasticity on particle-based drug delivery systems, Adv. Drug Deliv. Rev. 108 (2017) 51–67, http://dx.doi.org/10.1016/j.addr.2016.01.007.

[5] S. Sharma, H.I. Rasool, V. Palanisamy, C. Mathisen, M. Schmidt, D.T. Wong, J.K. Gimzewski, Structural-mechanical characterization of nanoparticle exosomes in human saliva, using correlative AFM, FESEM, and force spectroscopy, ACS Nano 4 (2010) 1921–1926, http://dx.doi.org/10.1021/nn901824n.

[6] W.-d. Tian, Y.-q. Ma, Theoretical and computational studies of dendrimers as delivery vectors, Chem. Soc. Rev. 42 (2013) 705–727, http://dx.doi.org/10.1039/C2CS35306G.

[7] B.S. Pattni, V.V. Chupin, V.P. Torchilin, New developments in liposomal drug delivery, Chem. Rev. 115 (2015) 10938–10966, http://dx.doi.org/10.1021/acs.chemrev.5b00046.

[8] M.J. Haney, N.L. Klyachko, Y. Zhao, R. Gupta, E.G. Plotnikova, Z. He, T. Patel, A. Piroyan, M. Sokolsky, A.V. Kabanov, E.V. Batrakova, Exosomes as drug delivery vehicles for Parkinson's disease therapy, J. Control. Release 207 (2015) 18–30, http://dx.doi.org/10.1016/j.jconrel.2015.03.033.

[9] Y. Hui, D. Wibowo, Y. Liu, R. Ran, H.-F. Wang, A. Seth, A.P.J. Middelberg, C.-X. Zhao, Understanding the effects of nanocapsular mechanical property on passive and active tumor targeting, ACS Nano 12 (2018) 2846–2857, http://dx.doi.org/10.1021/acsnano.8b00242.

[10] Y. Hui, X. Yi, F. Hou, D. Wibowo, F. Zhang, D. Zhao, H. Gao, C.-X. Zhao, Role of nanoparticle mechanical properties in cancer drug delivery, ACS Nano 13 (2019) 7410–7424, http://dx.doi.org/10.1021/acsnano.9b03924.

[11] G. Cevc, A. Chopra, Deformable (Transfersome®) vesicles for improved drug delivery into and through the skin, in: N. Dragicevic, H.I. Maibach (Eds.), Percutaneous Penetration Enhancers Chemical Methods in Penetration Enhancement: Nanocarriers, Springer, Berlin, 2016, pp. 39–59, http://dx.doi.org/10.1007/978-3-662-47862-2.

[12] D. Vorselen, S.M. van Dommelen, R. Sorkin, M.C. Piontek, J. Schiller, S.T. Döpp, S.A. Kooijmans, B.A. van Oirschot, B.A. Versluijs, M.B. Bierings, R. van Wijk, R.M. Schiffelers, G.J.L. Wuite, W.H. Roos, The fluid membrane determines mechanics of erythrocyte extracellular vesicles and is softened in hereditary spherocytosis, Nature Commun. 9 (2018) 4960, http://dx.doi.org/10.1038/s41467-018-07445-x.

[13] S. Ramachandran, A.P. Quist, S. Kumar, R. Lal, Cisplatin nanoliposomes for cancer therapy: AFM and fluorescence imaging of cisplatin encapsulation, stability, cellular uptake, and toxicity, Langmuir 22 (2006) 8156–8162, http://dx.doi.org/10.1021/la0607499.

[14] S. Li, F. Eghiaian, C. Sieben, A. Herrmann, I.A.T. Schaap, Bending and puncturing the influenza lipid envelope, Biophys. J. 100 (2011) 637–645, http://dx.doi.org/10.1016/j.bpj.2010.12.3701.

[15] O. Et-Thakafy, N. Delorme, C. Gaillard, C. Mériadec, F. Artzner, C. Lopez, F. Guyomarc'h, Mechanical properties of membranes composed of gel-phase or fluid-phase phospholipids probed on liposomes by atomic force spectroscopy, Langmuir 33 (2017) 5117–5126, http://dx.doi.org/10.1021/acs.langmuir.7b00363.

[16] D. Vorselen, F.C. MacKintosh, W.H. Roos, G.J. Wuite, Competition between bending and internal pressure governs the mechanics of fluid nanovesicles, ACS Nano 11 (2017) 2628–2636, http://dx.doi.org/10.1021/acsnano.6b07302.

[17] K. Johnson, Contact Mechanics, Cambridge University Press, Cambridge, 1985, http://dx.doi.org/10.1017/CBO9781139171731.

[18] W. Helfrich, Elastic properties of lipid bilayers: theory and possible experiments, Z. Naturforsch., C 28 (1973) 693–703, http://dx.doi.org/10.1515/znc-1973-11-1209.

[19] U. Seifert, R. Lipowsky, Adhesion of vesicles, Phys. Rev. A 42 (1990) 4768–4771, http://dx.doi.org/10.1103/PhysRevA.42.4768.

[20] E. Irajizad, A. Agrawal, Vesicle adhesion reveals novel universal relationships for biophysical characterization, Biomech. Model. Mechanobiol. 17 (2018) 103–109, http://dx.doi.org/10.1007/s10237-017-0947-x.

[21] X. Tang, J. Wang, X. Yi, Finite indentation of pressurized elastic fluid nanovesicles by a rigid cylindrical indenter, Acta Mech. Solida Sin. 32 (2019) 633–642, http://dx.doi.org/10.1007/s10338-019-00107-5.

[22] E. Boroske, M. Elwenspoek, W. Helfrich, Osmotic shrinkage of giant egg-lecithin vesicles, Biophys. J. 34 (1981) 95–109, http://dx.doi.org/10.1016/S0006-3495(81)84839-4.

[23] D.H. Boal, Mechanics of the Cell, second ed., Cambridge University Press, New York, 2012, http://dx.doi.org/10.1017/CBO9781139022217.

[24] C. de Boor, On calculating with B-splines, J. Approx. Theory 6 (1972) 50–62, http://dx.doi.org/10.1016/0021-9045(72)90080-9.

[25] S. Steltenkamp, C. Rommel, J. Wegener, A. Janshoff, Membrane stiffness of animal cells challenged by osmotic stress, Small 2 (2006) 1016–1020, http://dx.doi.org/10.1002/smll.200600018.

[26] A. Zdunek, A. Kurenda, Determination of the elastic properties of tomato fruit cells with an atomic force microscope, Sensors 13 (2013) 12175–12191, http://dx.doi.org/10.3390/s130912175.

[27] D. Vella, A. Ajdari, A. Vaziri, A. Boudaoud, The indentation of pressurized elastic shells: from polymeric capsules to yeast cells, J. R. Soc. Interface 9 (2011) 448–455, http://dx.doi.org/10.1098/rsif.2011.0352.

[28] Y. Lin, L. Freund, Forced detachment of a vesicle in adhesive contact with a substrate, Int. J. Solids Struct. 44 (2007) 1927–1938, http://dx.doi.org/10.1016/j.ijsolstr.2006.09.006.

[29] I.N. Sneddon, The relation between load and penetration in the axisymmetric boussinesq problem for a punch of arbitrary profile, Internat. J. Engrg. Sci. 3 (1965) 47–57, http://dx.doi.org/10.1016/0020-7225(65)90019-4.

[30] B. Cappella, G. Dietler, Force-distance curves by atomic force microscopy, Surf. Sci. Rep. 34 (1999) 1–104, http://dx.doi.org/10.1016/S0167-5729(99)00003-5.

[31] M.-G. Zhang, J. Chen, X.-Q. Feng, Y. Cao, On the applicability of Sneddon's solution for interpreting the indentation of nonlinear elastic biopolymers, J. Appl. Mech. 81 (2014) 091011, http://dx.doi.org/10.1115/1.4027973.

[32] X. Shi, Y.-P. Zhao, Comparison of various adhesion contact theories and the influence of dimensionless load parameter, J. Adhes. Sci. Technol. 18 (2004) 55–68, http://dx.doi.org/10.1163/156856104322747009.

[33] E. Schäfer, M. Vache, T.-T. Kliesch, A. Janshoff, Mechanical response of adherent giant liposomes to indentation with a conical AFM-tip, Soft Matter 11 (2015) 4487–4495, http://dx.doi.org/10.1039/C5SM00191A.

[34] F. Quemeneur, C. Quilliet, M. Faivre, A. Viallat, B. Pépin-Donat, Gel phase vesicles buckle into specific shapes, Phys. Rev. Lett. 108 (2012) 108303, http://dx.doi.org/10.1103/PhysRevLett.108.108303.

[35] S. Komura, K. Tamura, T. Kato, Buckling of spherical shells adhering onto a rigid substrate, Eur. Phys. J. E 18 (2005) 343, http://dx.doi.org/10.1140/epje/e2005-00038-5.

[36] M. Taffetani, D. Vella, Regimes of wrinkling in pressurized elastic shells, Philos. Trans. R. Soc., A 375 (2017) 20160330, http://dx.doi.org/10.1098/rsta.2016.0330.

[37] X. Yi, H. Gao, Cell membrane wrapping of a spherical thin elastic shell, Soft Matter 11 (2015) 1107–1115, http://dx.doi.org/10.1039/C4SM02427C.

[38] R. Dasgupta, R. Dimova, Inward and outward membrane tubes pulled from giant vesicles, J. Phys. D: Appl. Phys. 47 (2014) 282001, http://dx.doi.org/10.1088/0022-3727/47/28/282001.

[39] V. Heinrich, B. Božič, S. Svetina, B. Žekš, Vesicle deformation by an axial load: from elongated shapes to tethered vesicles, Biophys. J. 76 (1999) 2056–2071, http://dx.doi.org/10.1016/S0006-3495(99)77362-5.

[40] X. Yi, G. Zou, H. Gao, Mechanics of cellular packing of nanorods with finite and non-uniform diameters, Nanoscale 10 (2018) 14090–14099, http://dx.doi.org/10.1039/C8NR04110E.

[41] A.H. Deris, B. Nadler, Modeling the indentation and puncturing of inflated elastic membranes by rigid indenters, Int. J. Non-Linear Mech. 69 (2015) 29–36, http://dx.doi.org/10.1016/j.ijnonlinmec.2014.10.020.

[42] S.P. Pearce, J.R. King, T. Steinbrecher, G. Leubner-Metzger, N.M. Everitt, M.J. Holdsworth, Finite indentation of highly curved elastic shells, Proc. R. Soc. Lond. Ser. A Math. Phys. Eng. Sci. 474 (2018) 20170482, http://dx.doi.org/10.1098/rspa.2017.0482.

[43] G. Salbreux, G. Charras, E. Paluch, Actin cortex mechanics and cellular morphogenesis, Trends Cell Biol. 22 (2012) 536–545, http://dx.doi.org/10.1016/j.tcb.2012.07.001.

[44] H. Jiang, S.X. Sun, Cellular pressure and volume regulation and implications for cell mechanics, Biophys. J. 105 (2013) 609–619, http://dx.doi.org/10.1016/j.bpj.2013.06.021.

[45] M.R. Angle, A. Wang, A. Thomas, A.T. Schaefer, N.A. Melosh, Penetration of cell membranes and synthetic lipid bilayers by nanoprobes, Biophys. J. 107 (2014) 2091–2100, http://dx.doi.org/10.1016/j.bpj.2014.09.023.

[46] K. Yang, Y.-q. Ma, Computer simulation of the translocation of nanoparticles with different shapes across a lipid bilayer, Nat. Nanotechnol. 5 (2010) 579–583, http://dx.doi.org/10.1038/nnano.2010.141.

[47] H.-m. Ding, W.-d. Tian, Y.-q. Ma, Designing nanoparticle?translocation through membranes by computer simulations, ACS Nano 6 (2010) 1230–1238, http://dx.doi.org/10.1021/nn2038862.

[48] P. Rangamani, A. Agrawal, K.K. Mandadapu, G. Oster, D.J. Steigmann, Interaction between surface shape and intra-surface viscous flow on lipid membranes, Biomech. Model. Mechanobiol. 12 (2013) 833–845, http://dx.doi.org/10.1007/s10237-012-0447-y.

[49] M. Yu, R.B. Lira, K.A. Riske, R. Dimova, H. Lin, Ellipsoidal relaxation of deformed vesicles, Phys. Rev. Lett. 115 (2015) 128303, http://dx.doi.org/10.1103/PhysRevLett.115.128303.

[50] L. Liu, M. Yu, H. Lin, R. Foty, Deformation and relaxation of an incompressible viscoelastic body with surface viscoelasticity, J. Mech. Phys. Solids 98 (2017) 309–329, http://dx.doi.org/10.1016/j.jmps.2016.09.013.

[51] J. Wang, L. Li, Coupled elasticity–diffusion model for the effects of cytoskeleton deformation on cellular uptake of cylindrical nanoparticles, J. R. Soc. Interface 12 (2015) 20141023, http://dx.doi.org/10.1098/rsif.2014.1023.